The current issue and full text archive of this journal is available at
www.emeraldinsight.com/0961-5539.htm

A novel single domain approach for numerical modelling solid oxide fuel cells

A. Mauro
Dipartimento per le Tecnologie, Università degli Studi di Napoli "Parthenope", Napoli, Italy
F. Arpino
Dipartimento di Meccanica, Strutture, Ambiente e Territorio (DiMSAT), Università di Cassino, Cassino, Italy
N. Massarotti
Dipartimento per le Tecnologie, Università degli Studi di Napoli "Parthenope", Napoli, Italy, and
P. Nithiarasu
Civil and Computational Engineering Centre, School of Engineering, University of Wales Swansea, Swansea, UK

Received 24 December 2009
Accepted 2 February 2010

Abstract

Purpose – The purpose of this paper is to describe two- and three-dimensional numerical modelling of solid oxide fuel cells (SOFCs) by employing an accurate and stable fully matrix inversion free finite element algorithm.

Design/methodology/approach – A general and detailed mathematical model has been developed for the description of the coupled complex phenomena occurring in fuel cells. A fully matrix inversion free algorithm, based on the artificial compressibility (AC) version of the characteristic-based split (CBS) scheme and single domain approach have been successfully employed for the accurate and efficient simulation of high temperature SOFCs.

Findings – For the first time, a stable fully explicit algorithm has been applied to detailed multi-dimensional simulation transport phenomena, coupled to chemical and electrochemical reactions, in fluid, porous and solid parts of a SOFC. The accuracy of the present results has been verified via comparison with experimental and numerical data available in the literature.

Originality/value – For the first time, thanks to a stabilization analysis conducted, the AC-CBS algorithm has been successfully used to numerically solve the generalized model, applied in this paper to describe transport phenomena through free fluid channels and porous electrodes of SOFCs, without the need of further conditions at the fluid-electrode interface.

Keywords Numerical analysis, Modelling, Flow, Porosity, Energy supply systems
Paper type Research paper

Nomenclature

C_k k-sepcies molar concentration ($\mathrm{mol\,m^{-3}}$)

c_p specific heat ($\mathrm{kJ\,kg^{-1}\,K^{-1}}$)

D_K Knudsen diffusion coefficient ($\mathrm{m^2\,s^{-1}}$)

D_{kl} binary diffusion coefficient ($\mathrm{m^2\,s^{-1}}$)

D^e_{km} effective diffusion coefficient of species "k" in mixture "m" ($\mathrm{m^2\,s^{-1}}$)

D_{km} multicomponent diffusion coefficient ($\mathrm{m^2\,s^{-1}}$)

E Nernst cell potential (V)

E_O standard electrode potential (V)

E_a activation energy ($\mathrm{kJ\,mol^{-1}}$)

International Journal of Numerical Methods for Heat & Fluid Flow
Vol. 20 No. 5, 2010
pp. 587-612

0961-5539
DOI 10.1108/09615531011048268

F_o	Forchheimer coefficient
i	current density (A m^{-2})
I	cell current (A)
i_O	exchange current density (A m^{-2})
i_i	ionic current density (A m^{-2})
i_{avg}	average current density (A m^{-2})
j	species molar flux (mol m^{-2} s^{-1})
K	permeability (m^2)
k_e	electrolyte electrical conductivity (Ω^{-1} m^{-1})
M_k	k-species molecular weight (kg mol^{-1})
n_e	number of transferred electrons
p	pressure (Pa)
p_k	k-species partial pressure (Pa)
r_p	average pore size (μm)
S^e	energy source term (J m^3 s^{-1})
S_k	entropy of species k (J K^{-1})
S_k^m	k-species mass source term (kg m^{-2} s^{-2})
T	temperature (K)
u	velocity vector (m s^{-1})
$u_{\text{fuel,in}}$ and $u_{\text{air,in}}$	intel velocity
u_i	i-component of velocity vector (m s^{-1})
V_{ki}	k-species diffusion volume
X_k	k-species molar fraction
x_i	Cartesian i-coordinate (m)
y_k	k-species mass fraction

Greek symbols

α	charge transfer coefficient
γ	
ε	porosity
η_a	activation polarization (V)
η_c	concentration polarization (V)
η_{ohm}	ohmic polarization (V)
μ_e	effective dynamic viscosity (Pa s)
ρ	fluid density (kg m^{-3})
ρ_e	effective fluid density (kg m^{-3})
σ_e	electrolyte conductivity (S m^{-1})
σ_{kl}	diffusion collision diameter $\overset{o}{A}$
τ_g	tortuosity
Ω_{kl}	diffusion collision integral
ϑ	time (s)
μ	dynamic viscosity (Pa s)
δ_{ij}	Kronecker delta
ϕ	ionic potential (V)

Constants

F	Faraday constant (96,487 C mol^{-1})
R_g	universal gas constant (8.314 J mol^{-1} K^{-1})
π	pi (3.14159)

Subscripts

f	fluid region
s	solid region
b	bulk quantities
r	reaction site quantities

Superscripts

A	anodic quantities
C	cathodic quantities

1. Introduction

The importance to integrate the use of renewable energies with more efficient conversion of conventional fuels is compulsory in this time of increasing power demand, rising oil prices and environmental problems. Fuel cells are gaining popularity due to their high efficiency, cleanliness and cost-effective power supply

(Kirubakaran *et al.*, 2009). Although different fuel cell types are being investigated (Brandon and Thompsett, 2005; Sammes, 2006), solid oxide fuel cells (SOFCs) are considered very promising for stationary applications, due to a number of reasons, such as the modularity, fuel adaptability and very low levels of NO_x and SO_x emissions. The high operating temperatures (800-1,000 °C) allow cogeneration and the option of directly feeding hydrocarbons, such as natural gas, which can be reformed within the cell stack via catalyst materials (Aguiar *et al.*, 2004, 2005; Bae *et al.*, 2007; Bhattacharyya *et al.*, 2009; Cannarozzo *et al.*, 2007; Costamagna *et al.*, 2001; Hussian *et al.*, 2007; Palsson *et al.*, 2000; Riensche *et al.*, 2000; Singhal, 2000; Sundén and Faghri, 2005; Yakabe *et al.*, 2000; Xue *et al.*, 2005). This eliminates the need for external reformers. These features make SOFC technology particularly suitable for stationary, distributed power generation (Costamagna *et al.*, 2001; Palsson *et al.*, 2000; Riensche *et al.*, 2000). In hybrid SOFC-gas turbine power systems, pressurized SOFCs can be successfully used to increase electric efficiencies above 70 per cent (Singhal, 2000).

Over the years, many designs have been proposed for SOFCs. Since the 1960s, however, mainly planar and tubular designs have been developed (Sundén and Faghri, 2005). Lately, a number of researchers have started focusing on intermediate temperature solid oxide fuel cells (ITSOFCs) (Aguiar *et al.*, 2004, 2005; Bae *et al.*, 2007; Yakabe *et al.*, 2000), which operate at a temperature between 550 and 800 °C. Such ITSOFCs present more cost-effective fabrication and increased reliability, thanks to reduced thermal stresses. Nevertheless, due to the relatively thick electrodes employed in most anode-supported ITSOFCs, the development of these systems requires a detailed understanding of mass and energy transport phenomena, together with the electrochemical reactions occurring at the catalyst layer, which affect their performance (Bae *et al.*, 2007; Cannarozzo *et al.*, 2007; Greene *et al.*, 2006; Hussian *et al.*, 2007). Dynamic models have also been developed (Bhattacharyya *et al.*, 2009; Xue *et al.*, 2005) as important tools to be used for system optimization and dynamic control (Xue *et al.*, 2005), in order to increase the reliability of these systems.

Despite the intensive research and significant progress, SOFC technology is still at its prototype stage, mainly due to high manufacturing costs and low reliability. For SOFCs technology to become commercially available and therefore contribute to the solution of the present energy problem, a greater research effort is required to better understand some of the fundamental aspects of these devices. To achieve such goals, more efficient numerical models are needed, which should be able to accurately predict the behaviour of these systems in different operating load conditions. Nowadays, the trend in numerical modelling of SOFCs has started moving towards three-dimensional simulations, but the available literature shows that commercial codes are widely employed (Akhtar *et al.*, 2009; Danilov and Tade, 2009; Ho *et al.*, 2009; Lin *et al.*, 2007; Liu *et al.*, 2009), while non-commercial codes with dedicated algorithms are rare (Kapadia and Anderson, 2009). Furthermore, efficient parallelized codes are required to model fuel cells arranged in stacks (Kapadia and Anderson, 2009) and to solve problems with the required number of grid points.

Even though a number of numerical models have been proposed in the last few years for fuel cell simulations, a thorough analysis of the available literature shows that a detailed and robust modelling approach is still at its early stage of development (Ma *et al.*, 2005; Sammes, 2006; Singhal and Kendall, 2003; Sundén and Faghri, 2005). SOFCs can be examined as a heat and mass exchanger or as an electrochemical generator or as a chemical reactor or as a complete system by combining stacks with external devices such as reformers, contaminant removal units, compressors, etc. (Kakaç *et al.*, 2007). However, the models available in the literature are usually

classified in to two main categories as micro- and macro-models (Kakaç *et al.*, 2007). Most of the micro-models focus on the description of SOFC components, while macro-models mainly deal with the macroscopic or overall operational behaviours of SOFCs.

The models for numerical simulation of one cell form the basis for stack-level and eventually for system-level simulations. Among one cell macro-models, one of the earliest works was published in the 1980s by De Benedetti and Vayenas (1983), Vayenas *et al.* (1985). They considered a cross flow monolithic high temperature fuel cell as an electrochemical reactor in order to describe its behaviour under steady-state conditions. Later, a number of models appeared in the literature for the simulation of SOFCs (Bistolfi *et al.*, 1996; Costamagna, 1997; Ferguson *et al.*, 1996; Hirano *et al.*, 1992; Riess *et al.*, 1996; Standaert *et al.*, 1996). However, computational resources at the time did not allow researchers to couple the electrochemical models to the multidimensional transport phenomena simulation. Therefore, most of the initial multi-dimensional models introduced a number of simplifications to take into account the thermo-fluid dynamic aspects (Chan *et al.*, 2001; Chan and Xia, 2002; Riess *et al.*, 1996; Zhu and Kee, 2003).

More recently, advances in computational fluid dynamics (CFD) techniques have allowed researchers to use multi-dimensional and multi-component models for fuel cell simulations, mainly using commercial codes and finite volumes techniques (Autissier *et al.*, 2004; Beale *et al.*, 2003; Campanari and Iora, 2004; Khaleel *et al.*, 2004; Lockett *et al.*, 2004), even though the use of such commercial CFD tools may result in reduced flexibility, especially in overcoming some of the most common simplifying assumptions (Aguiar *et al.*, 2004; Lin and Beale, 2006; Yakabe *et al.*, 2000). It is also important to notice that the results obtained are rarely validated against experimental data, mainly because of lack of such data in the literature (Sundén and Faghri, 2005). In fact, attempts for validation of local mass transport phenomena are rarely available (Hecht *et al.*, 2005; Yakabe *et al.*, 2000).

For these reasons, the authors believe that it is important to develop a general, flexible and detailed numerical model in order to overcome the limitations of the existing fuel cell models. Moreover, the development of a robust model offers the possibility of using faster solution algorithms or numerical procedures, reducing the computational time and the resources required. This aspect is crucial in order to extend the model to a stack and system simulation level. The aim of the present work is to show how a stable and fully explicit matrix inversion free algorithm, based on the finite element method (FEM), can be successfully applied with a single domain approach, to accurately solve mass transport phenomena in a SOFC for the first time. The algorithm has been specifically developed by the authors in order to produce a stable, efficient and accurate solution for fluid dynamic, species concentration and current density distribution, also in presence of very high source terms, such as those due to low electrode permeability. Furthermore, quantities such as current density and diffusion coefficients are calculated locally and are not assumed to be constant.

In the past, the semi implicit (SI) version of the characteristic-based split (CBS) scheme was applied to the solution of SOFC problems (Arpino *et al.*, 2008), and a two domains approach was employed. Even though the previous work demonstrated the possibility to use the CBS algorithm for SOFC modelling, it appeared that the extension to 3D simulation needed a more efficient numerical procedure, which can easily be parallelized, implemented and needs few computational time for the solution process, especially in the presence of high source terms. For these reasons, a novel version of the CBS scheme has been specifically developed for the solution of complex and multidimensional fuel cell problems.

A new artificial compressibility (AC) version of the CBS algorithm is employed here for the first time for the simulation of fluid transport in SOFCs. The algorithm has been

recently applied to free fluid, saturated porous media and interface flow problems (Arpino *et al.*, 2009, 2010; Nithiarasu, 2003).

The present algorithm presents a number of advantages, as it allows an efficient simulation of fluid dynamic complex phenomena, especially in the presence of very large source terms. This is due to the stability analysis carried out in the recent past (Arpino *et al.,* 2010). The governing equations are solved via the FEM, which is the best choice for the solution of multidisciplinary problems, such as fuel cells. Furthermore, the AC-CBS algorithm is fully matrix inversion free and therefore particularly efficient in terms of computational requirements, and it can easily be parallelized. These are important requirements for a computational model in order to efficiently solve three-dimensional problems of fuel cells arranged in stacks, where millions of grid points are necessary.

The use of a single domain approach for the whole fuel cell increases the flexibility of the algorithm, as it is not necessary to impose boundary conditions (BCs) that are not known a priori.

The proposed model has been applied to two- and three-dimensional simulation of an anode-supported SOFC by employing a single domain approach. The results obtained in terms of mass transfer related phenomena have been successfully compared to the experimental data available in the literature (Yakabe *et al.*, 2000).

The paper is structured as follows: in section 2, the proposed mathematical model is presented; in section 3, the AC-CBS algorithm is described. The novel single domain approach is described in section 4 and the results obtained are given in section 5. In the last section, some conclusions are drawn.

2. Mathematical model

In the proposed mathematical model, the SOFC has been divided into three different components as depicted in Figure 1:

(1) anodic compartment, that includes fuel channel, porous anode and the anodic catalyst layer (interface between anode and electrolyte);

(2) ion-conducting electrolyte; and

(3) cathodic compartment, that includes oxidant channel, porous cathode and cathodic catalyst layer (interface between cathode and electrolyte).

The equations that describe the complex phenomena occurring inside a fuel cell include mass, momentum, species and energy conservation. In addition, other relations have to be considered in order to take into account all the specific electrochemical phenomena, such as the Nernst-Planck equation for the ideal electromotive force, the Butler-Volmer equation for the electrochemical kinetics and the Faraday equation which relates current density to reactant consumption/production.

The equations used in the present model have been derived on the basis of some assumptions, which are correctly used for the regimes described in this work:

- the fluid flow is incompressible;
- ideal gas behaviour;
- electrodes are saturated porous media with constant porosity and permeability;
- no electro-chemical reactions occur in the gas channels; and
- fuel cell operates under steady-state conditions.

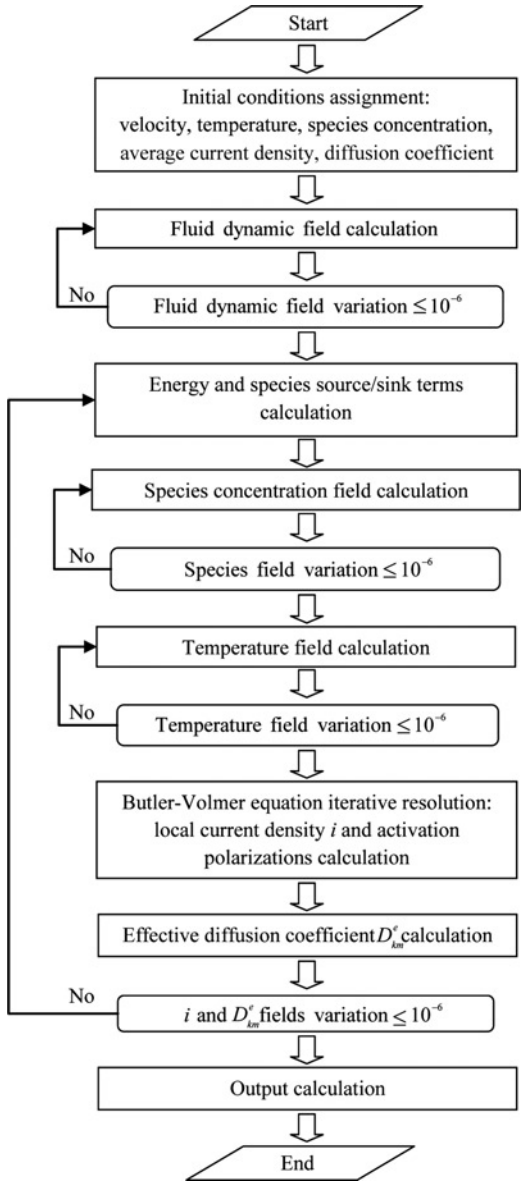

Figure 1.
Flow diagram of the proposed single domain fuel cell model

The quantities of interest in flow channels, porous electrodes, electrolyte and catalyst layers are therefore described by the equations presented in the following subsection.

2.1 The generalized porous medium model

Heat and fluid flow through fuel and oxidant channels and through porous electrodes is modelled by solving the generalized porous medium model (Arpino *et al.*, 2009; Massarotti *et al.*, 2001, 2003; Whitaker, 1961):

Mass conservation equation:

$$\frac{\partial u_j}{\partial x_j} = 0. \tag{1}$$

Momentum conservation equation:

$$\rho \frac{\partial u_i}{\partial \vartheta} + \frac{\rho}{\varepsilon} u_j \frac{\partial u_i}{\partial x_j} + \varepsilon \frac{\partial p}{\partial x_i} = \mu_e \frac{\partial}{\partial x_j}\left(\frac{\partial u_i}{\partial x_j}\right) - \frac{\mu \varepsilon u_i}{K} - \frac{\rho F_o \varepsilon |\mathbf{u}|}{\sqrt{K}}. \tag{2}$$

Energy conservation equation:

$$\varepsilon\left[(\rho c_p)_f + (1-\varepsilon)(\rho c_p)_s\right]\frac{\partial T}{\partial \vartheta} + (\rho c_p)_f \, u_i \frac{\partial T}{\partial x_i} - k_e \frac{\partial}{\partial x_i}\left(\frac{\partial T}{\partial x_i}\right) = S^e. \tag{3}$$

The subscript e in the equations above indicates the effective quanties in the porous domains (Arpino *et al.*, 2009; Massarotti *et al.*, 2001), while the negative source term on the right hand side (RHS) of Equation (2) takes into account the effect of the porous matrix.

The generalized porous medium model (Equations (1-3)) is particularly suitable for modelling partially porous domains. In fact, the Navier-Stokes equations can be obtained from the above generalized model equations by substituting $\varepsilon = 1$ and $K \to \infty$ to model the fuel and oxidant flow, while with $0 < \varepsilon < 1$ and $0 < K < \infty$, the porous matrix can be introduced, i.e. anode and cathode. The heat generated by the cell under operating conditions is accounted for using the energy source term S^e (Sundén and Faghri, 2005), on the RHS of Equation (3).

2.2 Mass transport

The transport of chemical species inside the fuel cell is governed by the following species conservation equation:

$$\varepsilon \rho_e \frac{\partial y_k}{\partial t} + \varepsilon \rho_e u_j \frac{\partial y_k}{\partial x_j} - \varepsilon \rho_e D^e_{km} \frac{\partial}{\partial x_j}\frac{\partial y_k}{\partial x_j} = S^m_k \tag{4}$$

where the subscript e for indicates the effective quantity in the porous domain (Arpino *et al.*, 2009; Massarotti *et al.*, 2001). The RHS includes the species source/sink term, S^m_k, of the species k in mixture m, which is derived from chemical reactions.

The calculation of the effective species diffusion coefficient for species k in mixture m, D^e_{km}, is crucial, as it directly affects the limiting fuel cell current, which corresponds to zero concentration values of reactant species at the reaction site (catalyst layers). In the absence of experimental data, several models are available in the literature for the calculation of the molecular diffusion coefficient on the basis of pressure, temperature and species concentration values. The most common method for theoretical estimation of gaseous diffusion is the one developed independently by Chapman and Enskog (Cussler, 1997; Perry *et al.*, 1997). This theory is based on a detailed analysis of molecular motion in diluted non-polar gases. The presence of the porous electrodes is taken into account through the Knudsen diffusion coefficient (Zhu and Kee, 2003) as:

$$D_K = \frac{4}{3} r_p \sqrt{\frac{8 R_g T}{\pi M_i}}. \tag{5}$$

The effective diffusion coefficient of species k in mixture m is then given by the following relation:

$$\frac{1}{D^e_{km}} = \frac{\tau_g}{\varepsilon}\left(\frac{1}{D_{km}} + \frac{1}{D_K}\right). \tag{6}$$

Since the exact value of tortuosity τ_g can be hardly evaluated, most codes in the literature use such parameter as a phenomenological fitting factor (Zhao and Virkar, 2005). In the present model, the tortuosity has been kept constant and equal to 4.5, in order to reproduce the same conditions that were used by the authors of the experimental data used here for validation (Yakabe *et al.*, 2000).

2.3 Electrochemical kinetics and fuel cell performance

Assuming the cell is fed by pure hydrogen and oxygen, the ideal electromotive force associated with electrochemical reactions is given by the well known Nernst equation (Singhal and Kendall, 2003):

$$E = E_0 - \frac{R_g T}{2F}\ln\left(\frac{p_{H_2O}}{p_{H_2} p_{O_2}^{0.5}}\right) \tag{7}$$

and the fluxes of reactants due to electrochemical reactions can be calculated according to Faraday's law (Singhal and Kendall, 2003):

$$j_k = \frac{i \cdot M_k}{n_e F}. \tag{8}$$

Under operating conditions, the cell voltage is lower than the Nernst voltage, as it is affected by losses (or overpotentials). These losses are mainly activation, concentration and ohmic overpotentials. The operating voltage is therefore calculated as:

$$V = E - \eta_a - \eta_c - \eta_{ohm}. \tag{9}$$

Activation losses η_a are related to the activation energy required by the chemical reactions. The relation between current density and activation overpotentials is governed by the phenomenological Butler-Volmer equation (Singhal and Kendall, 2003), which represents the net anodic and cathodic current due to an electrochemical reaction:

$$i = i_0\left[\exp\left(\alpha_A \frac{n_e F \eta_a}{R_g T}\right) - \exp\left(-\alpha_C \frac{n_e F \eta_a}{R_g T}\right)\right]. \tag{10}$$

The exchange current density i_0 at the electrode/electrolyte interface (catalyst layer), which appears in the above equation, is not simply a constant parameter. In fact, its value depends on the operating conditions and material properties, and also on fuel cell electrochemical reaction kinetics and reactants/products concentrations (Celik *et al.*, 2005). In the present model, the exchange current density has been evaluated on the basis of the relations available in Campanari and Iora (2004) and it is expressed by the following Arrhenius type equation:

$$i_0 = k_0 \exp\left(-\frac{E_a}{RT}\right). \tag{11}$$

When the cell is under no load (open circuit), the species concentrations at the reaction sites are the same as in the bulk channel flow, while under operating conditions there is a concentration gradient across the electrode structure, due to species mass fluxes that supply the electrochemical reactions. The difference in reactant and product concentrations between the bulk channel and the reaction site causes concentration losses, related to fuel and oxidant consumption in the cell. Such losses can then be evaluated as the difference between the Nernst potential in the bulk channel flow and the same quantity at the reaction sites, according to the following relation (Aguiar *et al.*, 2004; Campanari and Iora, 2004; Chan *et al.*, 2001; EG&G Technical Services, 2004; Greene *et al.*, 2006; Zhu and Kee, 2003):

$$\eta_c = \eta_c^A + \eta_c^C = \frac{R_g T}{2F} \ln\left(\frac{X_{H_2}^b X_{H_2O}^r}{X_{H_2}^r X_{H_2O}^b}\right) + \frac{R_g T}{4F} \ln\left(\frac{X_{O_2}^b}{X_{O_2}^r}\right). \tag{12}$$

The ohmic losses are due to the resistance to the ion flow in the electrolyte and the resistance to the electron flow in the electrodes. Since the electric current flow in both electrodes and electrolyte is governed by the Ohm's law, ohmic losses in planar SOFCs can be expressed by:

$$\eta_{ohm} = I \cdot R_i \tag{13}$$

where R_i represents the overall ohmic resistance, that is the sum of the cathode, electrolyte, anode, interconnect and contact ohmic resistance. Ohmic resistivities are usually calculated on the basis of an empirical formula of the type:

$$R_i = A \cdot \exp\left(\frac{B}{T}\right). \tag{14}$$

Typical values of specific resistance for SOFCs can be found in the literature (Li and Chyu, 2005; Nishino *et al.*, 2006; Stiller *et al.*, 2005).

2.4 Ion-conducting electrolyte

In a SOFC, the oxide ions (O^{2-}), throughout an ion conducting electrolyte, migrate from the air electrode (cathode) side to the fuel electrode (anode) side, where they react with the fuel (H_2, CO, etc.) to generate an electrical voltage. Under stationary operating conditions, the migration of oxide ions is governed by the following equation:

$$\nabla \cdot i_i = 0. \tag{15}$$

Using Ohm's law, the ionic current density can be related to the ionic potential and Equation (15) becomes:

$$k_e \nabla^2 \phi = 0. \tag{16}$$

From the thermal point of view, heat transfer inside the electrolyte is governed by the following equation (Singhal and Kendall, 2003):

$$\lambda_e \nabla^2 T = \sigma_e (\nabla \phi \cdot \nabla \phi). \tag{17}$$

3. The artificial compressibility characteristic-based split algorithm

A three-dimensional finite element code based on the AC-CBS algorithm has been developed to solve the coupled partial differential equations (PDEs) employed in the presented model. The AC-CBS procedure has been successfully applied to the solution of free fluid, saturated porous media and interface flow problems (Arpino *et al.*, 2009, 2010; Nithiarasu, 2003).

The governing PDEs have been discretized in time along the characteristics, and in space using the standard Galerkin procedure (Arpino *et al.*, 2009; Zienkiewicz *et al.*, 2005). The temporal discretization along the characteristics leads to the introduction of higher order convective terms, while the splitting of velocity and pressure leads to three separate steps in the solution procedure (Arpino *et al.*, 2009; Zienkiewicz *et al.*, 2005). The three steps of the AC-CBS algorithm can be written as:

(1) Intermediate velocity calculation:

$$\begin{aligned} \tilde{u}_i^{n+1}(1 + \Delta t \varepsilon P \vartheta_3) - u_i^n (1 - \Delta t \varepsilon P (1 - \vartheta_3)) = & -\left[\frac{\Delta t}{\varepsilon} u_j \frac{\partial u_i}{\partial x_j}\right]^n \\ & + \left[\Delta t \frac{\mu_e}{\rho_f} \frac{\partial^2 u_i}{\partial x_i^2}\right]^n + \varepsilon \frac{\Delta t^2}{2} \left[\frac{1}{\varepsilon^2} u_k \frac{\partial}{\partial x_k}\left(u_j \frac{\partial u_i}{\partial x_j}\right)\right]^n . \end{aligned} \tag{18}$$

(2) Pressure calculation:

$$\frac{1}{\beta^2}(p^{n+1} - p^n) = -\Delta t \frac{\rho_f}{\varepsilon}\left(\vartheta_1 \frac{\partial \tilde{u}_i^{n+1}}{\partial x_i} + (1 - \vartheta_1)\frac{\partial u_i^n}{\partial x_i}\right) + \Delta t^2 \frac{\partial^2 p^n}{\partial x_i^2}. \tag{19}$$

(3) Velocity correction:

$$(1 + \varepsilon \Delta t P \vartheta_3)(u_i^{n+1} - \tilde{u}_i^{n+1}) = -\varepsilon \Delta t \left[\vartheta_2 \frac{\partial p^{n+1}}{\partial x_i} + (1 - \vartheta_2)\frac{\partial p^n}{\partial x_i} + \left(\frac{\Delta t}{2} u_k \frac{\partial}{\partial x_k}\frac{\partial p}{\partial x_i}\right)^n\right] \tag{20}$$

where $0.5 \leq \vartheta_1 \leq 1$ and $0 \leq \vartheta_i \leq 1$, with $i = 2, 3$. For the AC scheme employed in the present study, $\vartheta_1 = 1 \text{and} \vartheta_2 = \vartheta_3 = 0$. In the above equations, velocity, pressure and temperature are artificial quantities while iterating. This is due to the fact that the incompressibility constraint is not enforced at each time step. When steady-state convergence is reached, actual quantities are obtained (Arpino *et al.*, 2009). The superscripts $n + 1$ and n refer to the iterative procedure and not to actual time levels. The term $P = (\mu_e \varepsilon / \rho K) + (F_0 \varepsilon |\mathbf{u}| / \sqrt{K})$ takes into account the presence of the porous matrix. A stability analysis has been recently carried out for the present AC-CBS algorithm, obtaining a robust and efficient fully explicit matrix inversion

free procedure for the solution of saturated porous media and free fluid interface flow problems (Arpino *et al.,* 2010).

Depending on the problem of interest, it is possible to consider other equations coupled to the above set, such as:

(4) Temperature field calculation:

$$T^{n+1} - T^n = \Delta t \frac{(\rho c_p)_f}{\varepsilon(\rho c_p)_f + (1-\varepsilon)(\rho c_p)_s}\left[-u_i\frac{\partial T}{\partial x_i} + \frac{\lambda}{(\rho c_p)_f}\frac{\partial^2 T}{\partial x_i^2}\right]^n + \frac{\Delta t^2}{2}\frac{(\rho c_p)_f}{\varepsilon(\rho c_p)_f + (1-\varepsilon)(\rho c_p)_s}\left[\bar{u}\frac{\partial}{\partial x_j}\left(u_i\frac{\partial T}{\partial x_i}\right)\right]^n. \quad (21)$$

(5) Species field calculation:

$$\rho_e(y_k^{n+1} - y_k^n) = \Delta t\left[-\rho_e u_j\frac{\partial y_k}{\partial x_j} + \rho_e D_{km}^e\frac{\partial y_k}{\partial x_i}\right]^n + \frac{\Delta t^2}{2}\left[\bar{u}\frac{\partial}{\partial x_j}\left(\rho_e D_{km}^e\frac{\partial y_k}{\partial x_i}\right)\right]^n. \quad (22)$$

The above equations are discretized in space using the standard Galerkin finite element procedure (Zienkiewicz *et al.*, 2005). The three-dimensional computational domain is subdivided into a tetrahedral mesh of finite elements. Within the elements each variable is approximated by a linear function that can be expressed in terms of its value at the four nodes of a tetrahedral element:

$$\phi = \sum_{n=1}^{4} N_n\bar{\phi}_n \quad (23)$$

where N_n is the shape function and $\bar{\phi}_n$ is the value of the generic approximated variable ϕ at node n. The equations obtained substituting the approximated function in Equations (18)-(22) are then weighted using the same shape function, N_n, and integrated over the computational domain.

4. The proposed single domain fuel cell solution procedure

The dependence of species diffusion coefficients and local current density distribution on velocity, species and temperature fields requires an iterative process for the resolution of the proposed fuel cell model. Assuming that the electrochemical reactions do not significantly affect the mixture thermodynamic properties (density, viscosity, etc.), energy and species conservation equations are solved afterwards the pressure and velocity fields determination. The continuity of temperature, electric current and potential at the interfaces between porous electrodes and electrolyte make desirable a single domain approach for the modelling of the entire fuel cell. In such a way, no further conditions are required at the interfaces between the different sub-domains. The resolution procedure adopted in this work is relative to the isothermal case and can be summarized by the following main steps:

(1) resolution of mass and momentum conservation equations for the determination of pressure and velocity fields;

(2) guess an initial distribution for local current density and effective species diffusion coefficients;

(3) calculation of reactants fluxes at the catalyst layer according to Equation (8);

(4) resolution of species conservation equation;

(5) resolution of Butler-Volmer equation for the calculation of new current density distribution at the catalyst layer;

(6) calculation of new species effective diffusion coefficients; and

(7) restart form step "(3)" until convergence on local current density distribution and species diffusion coefficient fields is reached.

Once the global convergence is reached, the concentration polarizations are evaluated and, finally, the fuel cell performances are determined in terms of operative cell voltage and cell power density. More details about the proposed resolution process can be derived from Figure 1.

5. Results

In the present work, a planar anode-supported SOFC is modelled. Different fuel cell components, together with the BCs employed for the simulations, are shown in Figure 2. The BCs employed for the fluid dynamic field, modelled by Equations (1) and (2) are as follows. The velocity distribution is assigned at the inlet section, while, at the outlet section, pressure is assigned (see Figure 2). A no slip BC is assigned to the top and bottom horizontal walls. Symmetry velocity BCs are assigned to the vertical side walls. Temperature is assigned at the inlet section, adiabatic walls are assumed at the top and bottom of the computational domain, while at the outlet section, natural BC is assigned. Symmetry temperature BCs are assigned to the vertical side walls. The BCs employed for the species concentration field, modelled by Equation (4), are: species concentrations are assigned at the inlet section of fuel and air channels, while reactants/products, consumption/production due to electrochemical reactions is modelled as an assigned mass flux at the catalyst layer, i.e. reaction site (red face in Figure 2), according to Faraday's law. The top and bottom horizontal walls are considered impermeable to mass. In the absence of experimental data, the binary diffusion coefficients have been theoretically estimated according to the Chapman and Enskog theory (Cussler, 1997; Perry *et al.*, 1997). The effective diffusion coefficient of species k in mixture m for the porous medium is calculated according to Equations (5) and (6).

The results for 2D simulations of the anode-supported planar SOFC, considered in the present work, have been obtained by employing a structured computational grid refined

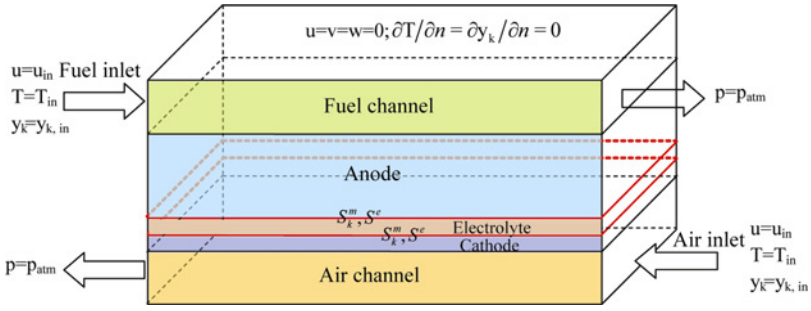

Figure 2.
Schematic representation and BCs employed for the simulation of a planar anode-supported SOFC

near the top and bottom walls and at the interfaces between the three different subdomains. The mesh employed, shown in Figure 3, contains 5,589 nodes and 10,560 triangular elements, and it has been determined on the basis of a mesh sensitivity analysis. In order to verify the algorithm in three dimensions, an unstructured computational grid refined near the top and bottom walls and at the interfaces between the three different subdomains has been used. The mesh employed contains 62,211 nodes and 252,491 tetrahedral elements. This mesh was generated using the PSUE, available within the School of Engineering, Swansea University (Morgan *et al.*, 1999), and a detail of it near the fuel entrance is shown in Figure 4.

The proposed model has been verified by simulating mass transfer phenomena in an isothermal planar anode-supported SOFC, fed by a mixture of H_2, H_2O and Ar, for which experimental data are available in literature (Yakabe *et al.*, 2000). Since the generalized porous medium model is employed to describe the energy and mass transport phenomena in the anodic and cathodic compartments, no further BCs are needed at the interface between free fluid channels and porous electrodes. The comparison with experimental data is carried out on the basis of concentration polarizations in the anodic compartment of the fuel cell. The parameters adopted for the present simulations were extracted from the experimental data of Yakabe *et al.* (2000) and are listed in Table I. As the physical parameters are available only for the anode, the quantities listed in Table I are employed for both electrodes. As the order of magnitude of such parameters is the

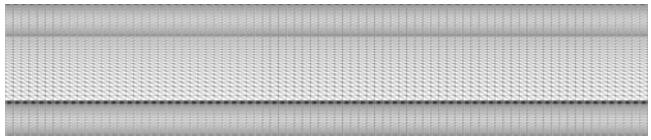

Figure 3.
Two-dimensional computational grid employed: 5,589 nodes and 10,560 triangular elements

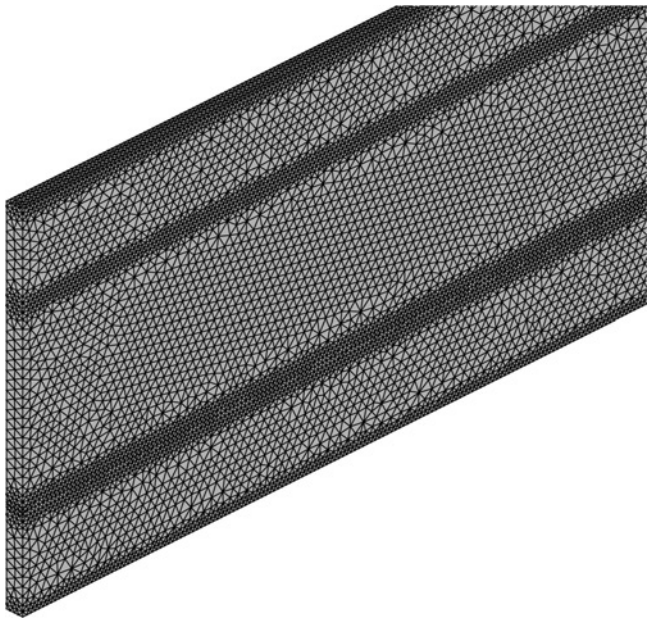

Figure 4.
Three-dimensional computational grid employed: 62,211 nodes and 252,491 tetrahedral elements

Parameter	Symbol	Value
Operating temperature (K)	T	1,023
Operating pressure (atm)	P	1.0
Inlet fuel velocity (m/s)	u_{in}	2.0
Inlet air velocity (m/s)	u_{in}	2.0
Current density (A/cm^2)	i_{avg}	0.30, 0.70
Porosity	ε	0.46
Average pore size (μm)	r_p	2.6
Tortuosity	τ_g	4.5
Anode permeability (m^2)	η^A	1.76×10^{-11}
Anode thickness (mm)		2.0

Source: Yakabe *et al.* (2000)

Table I.
Physical properties of cell electrodes and input parameters

same for anode and cathode (Chan *et al.*, 2001; Chan and Xia, 2002; Hussian *et al.*, 2007), and the cathode is two order of magnitude thinner than the anode, this assumption is not expected to affect the results obtained. The assigned inlet velocity of the fuel is 2.0 m/s that corresponds to a calculated fuel utilization (FU) factor less than 5 per cent, which is close to the experimental condition (Yakabe *et al.*, 2000).

Figure 5 shows a comparison in terms of concentration overpotentials, η_c^A, of the results obtained with the present algorithm with the experimental and numerical data from Yakabe *et al.* (2000). The comparison is performed for average current density values of 0.3 A/cm^2 and 0.7 A/cm^2. The reactants concentration is reported on the horizontal axis. The reference value on the vertical axis, η_{c0}^A, is calculated at $H_2/(H_2 + H_2O + Ar) = 0.8$. The ratio of H_2/H_2O is kept at 80/20 and the concentration of H_2 in the system is varied by the degree of dilution of the inlet fuel with Argon. Therefore, η_{c0}^A is calculated when no argon is present in the system.

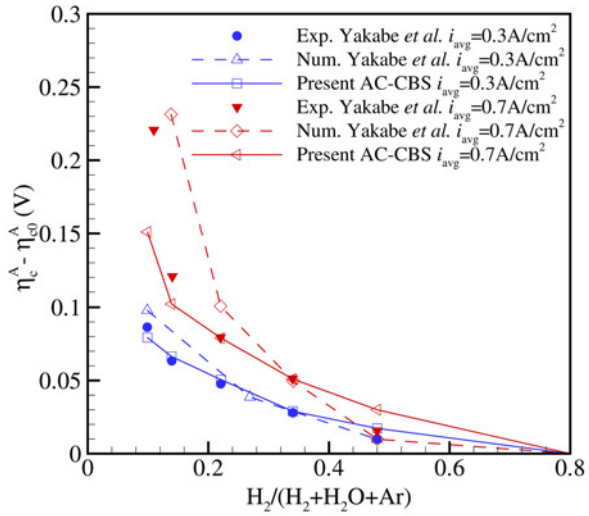

Note: Comparison with the experimental and numerical data available in Yakabe *et al.* (2000)

Figure 5.
Concentration overpotentials for the H_2-H_2O-Ar fuel mixture, at $i_{avg} = 0.3$ A/cm^2 and $i_{avg} = 0.7$ A/cm^2

The results shown in Figure 5 are the same in both two and three dimensions, since the simulations performed by using the 3D AC-CBS code have been carried out by employing symmetry BCs for the vertical side walls of the computational domain. Figure 5 shows that η_c^A increases as H_2 concentration at the inlet mixture decreases. This behaviour is more rapidly for low reactant concentration. In terms of current density, it can be noticed from the same figure that for higher current densities, which correspond to higher fuel consumption, concentration overpotentials increase. This can be explained as follows. At high fuel concentration and low operating current densities, the bulk gas contains sufficient reactant to diffuse easily through the electrode to the anode-electrolyte interface, where the low reactant consumption produces small reactant concentration gradients across the electrode. This results in low η_c^A. On the other hand, for low inlet fuel concentration and high operating current density, the amount of reactant in the bulk gas is not sufficient to attain the desired operating current density. This results in higher concentration gradients across the anode and starvation of reactants at the reaction site.

From the analysis of Figure 5, it can be noticed that for both mean current density values considered, the numerical solution agrees very well with experimental data, particularly at $i_{avg} = 0.3\ \mathrm{A/cm^2}$. For both cases considered, the numerical results slightly overestimate the experimental data at low dilution factors, and slightly underestimate the experimental data when fuel is highly diluted with argon. The present calculations show a significantly better approximation of the experimental data respect to the numerical results that the authors of the experiment predicted (Yakabe *et al.*, 2000).

5.1 Fuel cell performance evaluation

The fuel cell performance, in terms of operative voltage and power density, has been evaluated assuming that a mixture of gas at the constant temperature of 1,023 K with a constant mass ratio $H_2/H_2O = 80/20$ is introduced at the fuel inlet. The domain temperature is also kept constant at 1,023 K. Such assumption is acceptable since the anode-supported SOFC was placed inside an alumina tube in a furnace which allowed the control of the SOFC temperature distribution (Yakabe *et al.*, 2000). In order to reproduce a wide range of FU factors, three different fuel inlet velocities are simulated: $2.81 \times 10^{-1}\ \mathrm{m/s}$, corresponding to a FU factor between 1.5 per cent at $i_{avg} = 0.1\ \mathrm{A/cm^2}$ and 10 per cent at $i_{avg} = 0.7\ \mathrm{A/cm^2}$; $8.45 \times 10^{-2}\ \mathrm{m/s}$, corresponding to a FU factor between 5.0 per cent at $i_{avg} = 0.1\ \mathrm{A/cm^2}$ and 35 per cent at $i_{avg} = 0.7\ \mathrm{A/cm^2}$; $5.00 \times 10^{-2}\ \mathrm{m/s}$, corresponding to a FU factor between 8.5 per cent at $i_{avg} = 0.1\ \mathrm{A/cm^2}$ and 60 per cent at $i_{avg} = 0.7\ \mathrm{A/cm^2}$. For all the studied cases, the air inlet velocity is assumed to be 1.0 m/s.

Figure 6 shows the fuel and oxidant horizontal velocity field in the fuel cell, at a fuel inlet velocity of $2.81 \times 10^{-1}\ \mathrm{m/s}$. Since the thickness of cathode and electrolyte (0.05 mm) is about two orders of magnitude smaller than the anode (2 mm) and the channels (1 mm), these domains are not clearly visible in the figure. It is evident from the figure that the velocity decreases rapidly in the anode, because of the very low permeability. The velocity magnitude in the porous electrodes is of the order of 10^{-5} m/s, while a maximum velocity of 1.5 m/s in the air channel and 0.42 m/s in the fuel channel have been calculated. The solution shown in Figure 6, obtained when the residuals were below 10^{-6}, required less than 3 hours on a machine with 2.4 GHz processor and 4 Gb Ram. It has been possible to obtain such results, thanks to the AC-CBS stability analysis recently carried out (Arpino *et al.,* 2010).

Figures 7-9 present the hydrogen (a) and oxygen (b) mass fraction distributions in the anodic and cathodic compartments at a mean current density value $i_{avg} = 0.2\ \mathrm{A/cm^2}$. The fuel inlet velocities used in these figures are $2.81 \times 10^{-1}\ \mathrm{m/s}$, $8.45 \times 10^{-2}\ \mathrm{m/s}$ and

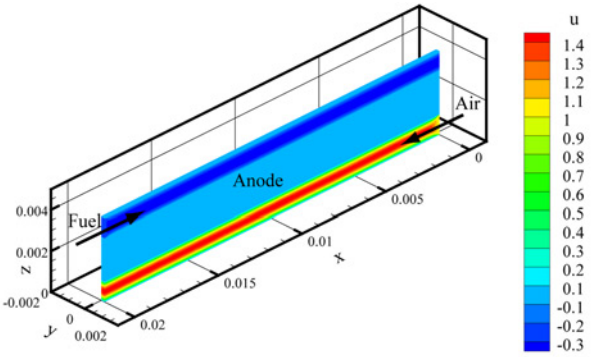

Notes: Fuel inlet velocity $u_{in} = 2.81 \times 10^{-1}$ m/s; air inlet velocity $u_{fuel,\ in}$ and $u_{air,\ in} = 1.0$ m/s

Figure 6.
Horizontal velocity field in the fuel cell

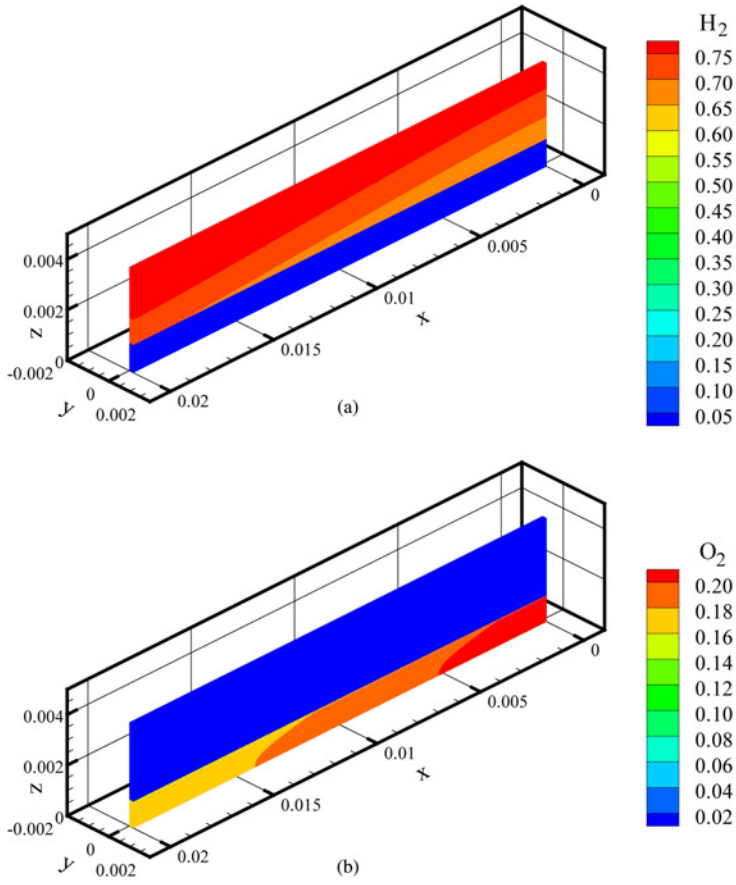

Figure 7.
Hydrogen (a) and oxygen (b) mass fraction distribution in the fuel cell, for an average current density $i_{avg} = 0.2$ A/cm^2 and a fuel inlet velocity $u_{fuel,\ in}$ and $u_{air,\ in} = 2.81 \times 10^{-1}$ m/s

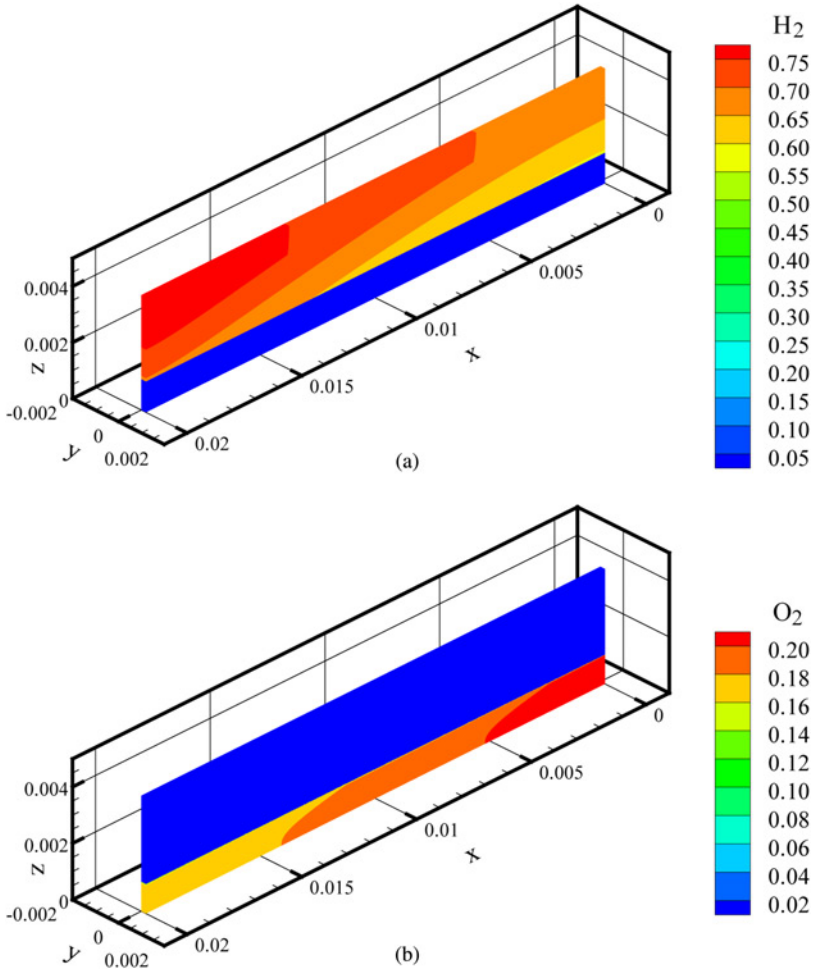

Figure 8.
Hydrogen (a) and oxygen (b) mass fraction distribution in the fuel cell, for an average current density $i_{avg} = 0.2$ A/cm^2 and a fuel inlet velocity $u_{\text{fuel, in}}$ and $u_{\text{air, in}} = 8.45 \times 10^2$ m/s

5.00×10^{-2} m / s, respectively. From these figures, it is evident that the fuel inlet velocity significantly modifies the H_2 and O_2 concentration fields, since it directly affects the FU factor. In particular, the mass fraction distribution calculated at the catalyst layers at the maximum fuel inlet velocity (Figure 9) varies along the fuel cell, while at the minimum fuel inlet velocity a more homogeneous fuel mass fraction distribution is found at the catalyst layer (Figure 7). As expected, the minimum hydrogen mass fraction at the catalyst layer was found at the minimum fuel inlet velocity, i.e. maximum FU factor. The oxygen concentration does not vary for these three cases, as expected.

Figures 10-12 present the hydrogen (a) and oxygen (b) mass fraction distributions in the anodic and cathodic compartments at a mean current density value $i_{avg} = 0.4$ A/cm^2. In this case, the same fuel inlet velocities used in Figures 7-9 are considered, respectively, for the results of Figures 10-12. From these figures, it is clear that the behaviour of the

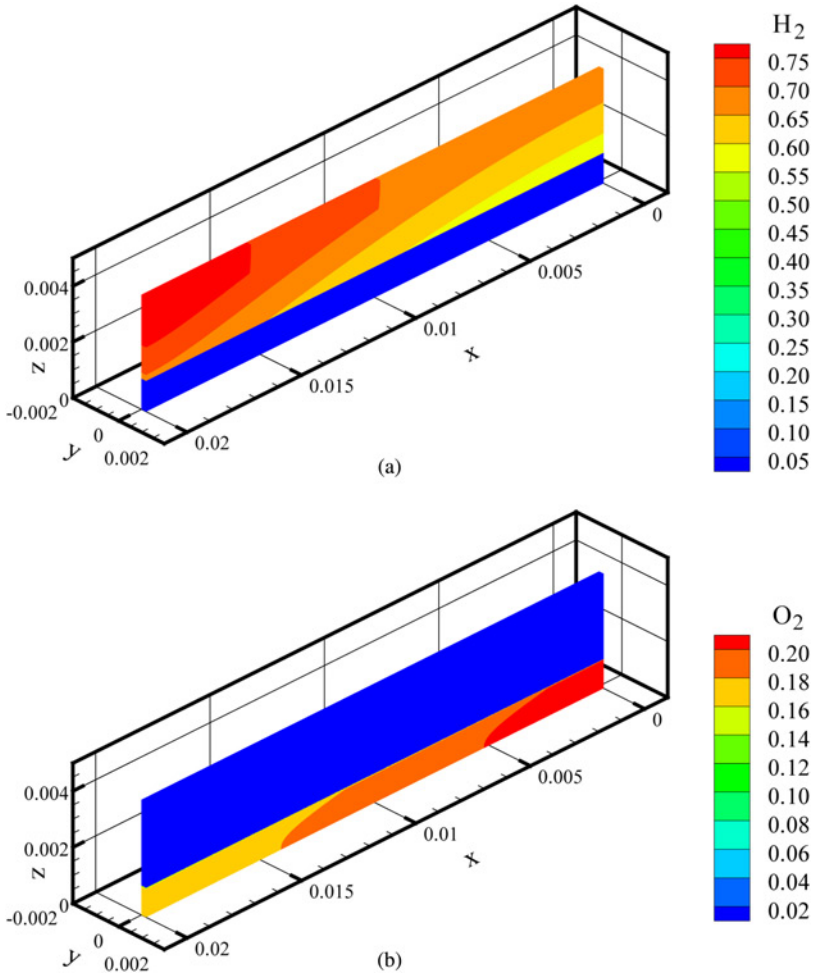

Figure 9.
Hydrogen (a) and oxygen (b) mass fraction distribution in the fuel cell, for an average current density $i_{avg} = 0.2$ A/cm^2 and a fuel inlet velocity $u_{\text{fuel, in}}$ and $u_{\text{air, in}} = 5.00 \times 10^{-2}$ m/s

cell is similar, but the variation of fuel concentration along the fuel cell is increased respect to the lower current density of the previous case. The comparison between the mass fraction distributions at $i_{avg} = 0.2$ A/cm^2 and $i_{avg} = 0.4$ A/cm^2 also shows that a higher current density corresponds to higher consumption of oxygen inside the fuel cell.

Since the minimum fuel mass fraction at the catalyst layer corresponds to the maximum concentration losses, the inlet fuel velocity also affects the fuel cell limiting current density. This is clearly shown in Figure 13, which presents the anodic and cathodic concentration losses as a function of the average cell current density at different fuel inlet velocities considered. This figure shows a significant increment in both anodic and cathodic concentration overpotentials for higher values of the mean current density. This is due to the higher fuel consumption rate at higher values of cell current density. Figure 13 also shows that the anodic concentration polarizations do not vary significantly, at lower current densities, with the fuel inlet velocity. However, these

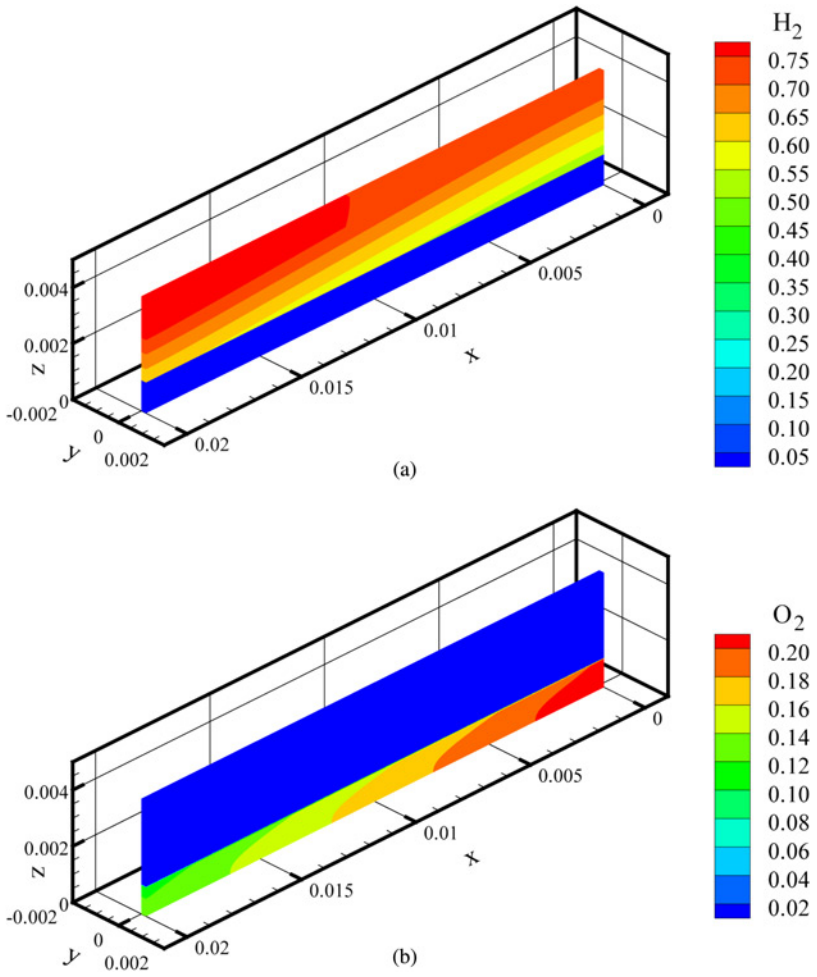

Figure 10.
Hydrogen (a) and oxygen (b) mass fraction distribution in the fuel cell, for an average current density $i_{avg} = 0.4$ A/cm^2 and a fuel inlet velocity $u_{\text{fuel, in}}$ and $u_{\text{air, in}} = 2.81 \times 10^{-1}$ m/s

differences become important for higher values of the average current density. As the cathodic concentration losses are concerned, it is evident that they have less influence on the performance of the anode-supported fuel cell considered in the present work.

Figure 14 shows the ohmic losses and both anodic and cathodic activation overpotentials as a function of the average cell current density, for different values of the mean cell current density. Since the air inlet parameters are kept constant at the cathodic compartment, no differences can be noticed as the fuel inlet velocity changes. It can be observed that both the anodic and cathodic activation losses are much smaller than the ohmic activation losses and do not influence significantly the cell performance, both in terms of output power density and operative voltage. The ohmic polarization, calculated on the basis of Equation (13), presents a linear behaviour as

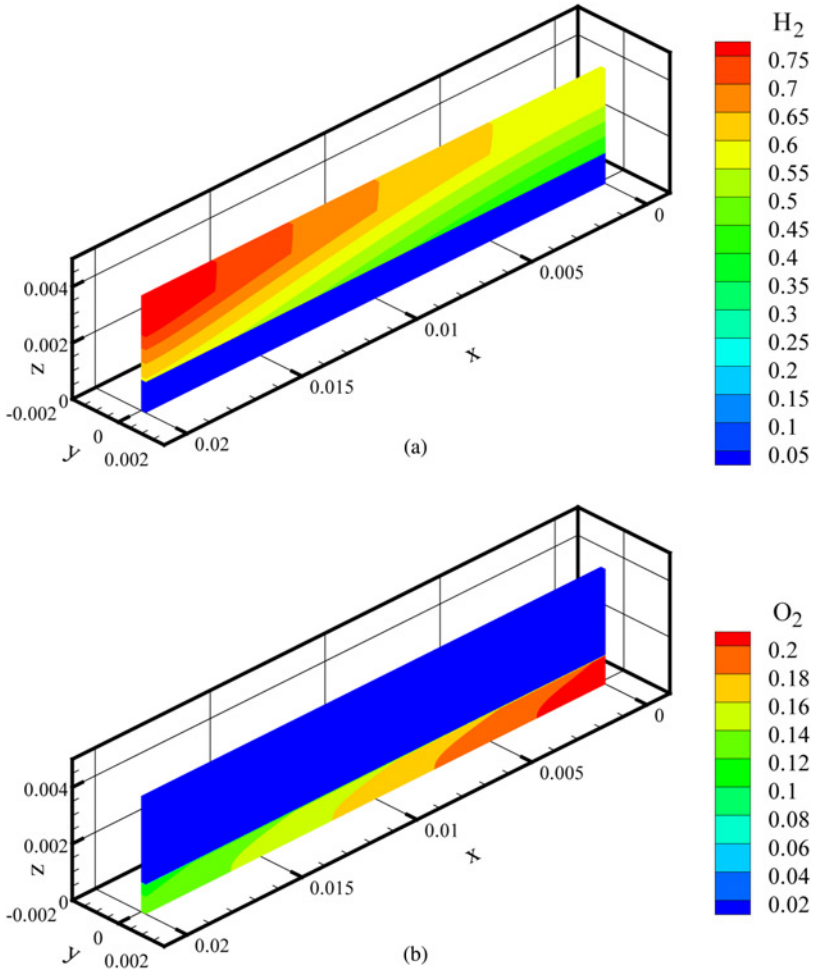

Figure 11.
Hydrogen (a) and oxygen (b) mass fraction distribution in the fuel cell, for an average current density $i_{avg} = 0.4$ A/cm^2 and a fuel inlet velocity $u_{\text{fuel, in}}$ and $u_{\text{air, in}} = 8.45 \times 10^{-2}$ m/s

expected. The calculation of ionic and electronic resistances of the different parts of the fuel cell is based on the data available from the literature (Stiller *et al.*, 2005).

Figure 15 presents the operative cell voltage and the cell power density, for the three fuel inlet velocities considered, as a function of the average current density. As the FU factor increases, i.e. fuel inlet velocity decreases, the peak in the power density of the fuel cell decreases and moves slightly towards lower average current density values. Furthermore, for higher FU factors, there is a faster drop in the cell power density at the peak cell current density. This is due to the higher fuel consumption rate at higher values of cell current density, that causes a rapid increase in the concentration losses (Figure 13). In fact, from the analysis of Figures 13-15, it can be noticed that both anodic and cathodic concentration losses significantly increase for higher values of the mean cell current density and they are responsible of the rapid drop in the cell voltage

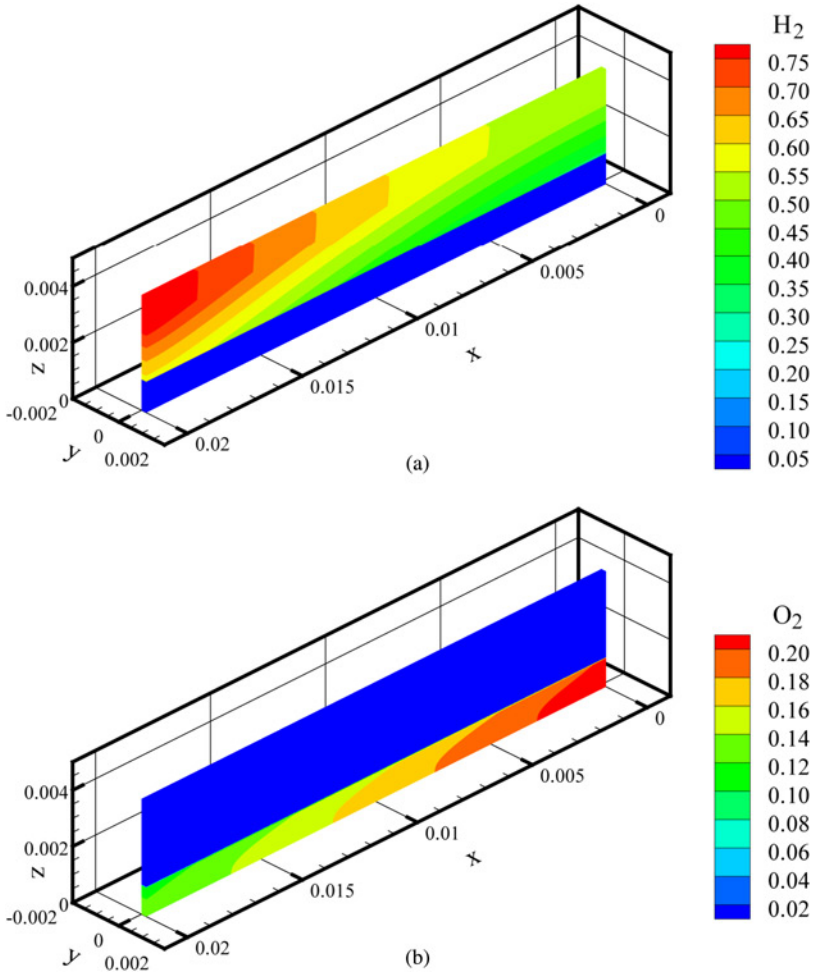

Figure 12.
Hydrogen (a) and oxygen (b) mass fraction distribution in the fuel cell, for an average current density $i_{avg} = 0.4$ A/cm^2 and a fuel inlet velocity $u_{\text{fuel, in}}$ and $u_{\text{air, in}} = 5.00 \times 10^{-2}$ m/s

when the maximum cell current is approached. Obviously, the cell power density decreases accordingly.

6. Conclusions

In the present paper, a matrix inversion free method, based on the AC-CBS scheme, has been employed for the 2D and 3D simulation of the complex coupled phenomena occurring in an anode-supported high temperature SOFC. The generalized porous medium approach has been employed to simulate transport phenomena in free fluid channels and porous electrodes. A novel single domain approach has been used for the whole fuel cell, in conjunction with a stable AC version of the CBS algorithm, increasing the flexibility of the model proposed in the present paper, respect to the previous version of the CBS. The overall fuel cell performance has been analysed for

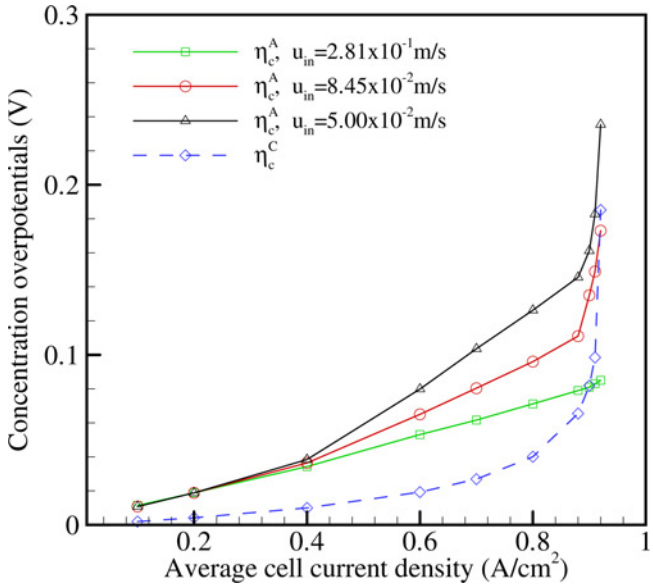

Figure 13.
Anodic and cathodic concentration overpotentials as function of the mean cell current density, for different values of fuel inlet velocity

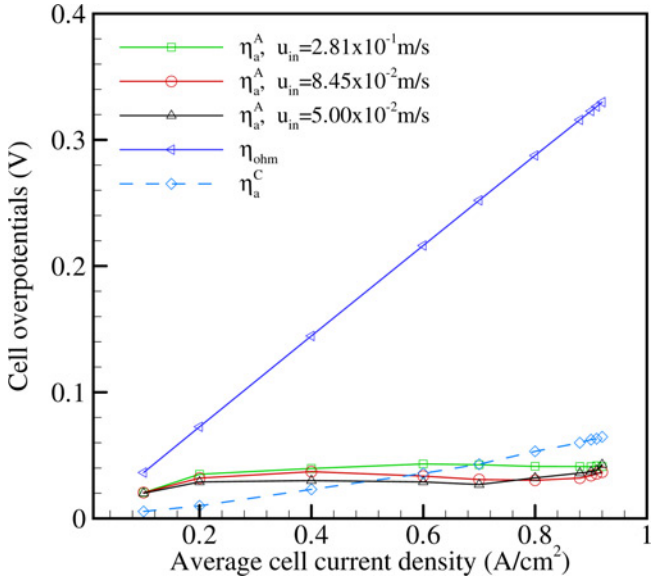

Figure 14.
Ohmic losses and both anodic and cathodic activation overpotentials as function of the average cell current density, for different values of fuel inlet velocity

different FU factors. The present results have been verified, both in two and three dimensions, through comparison with experimental and numerical data available in the literature. The authors believe that the present matrix inversion free algorithm, thanks to the stability analysis developed and to the single domain approach employed, is a very promising variant for detailed 3D simulations of SOFC performance.

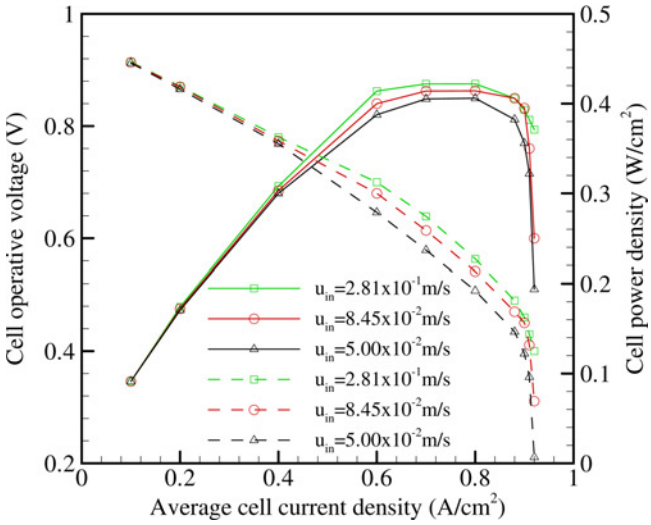

Figure 15.
Cell operative voltage and cell power density as function of the average cell current density, for different values of fuel inlet velocity

References

Aguiar, P., Adjiman, C.S. and Brandon, N.P. (2004), "Anode-supported intermediate-temperature direct internal reforming solid oxide fuel cell II. Model-based steady-state performance", *Journal of Power Sources*, Vol. 138, pp. 120-36.

Aguiar, P., Adjiman, C.S. and Brandon, N.P. (2005), "Anode-supported intermediate-temperature direct internal reforming solid oxide fuel cell II. Model-based dynamic performance and control", *Journal of Power Sources*, Vol. 147, pp. 136-47.

Akhtar, N., Decent, S.P., Loghin, D. and Kendall, K. (2009), "A three-dimensional numerical model of a single-chamber solid oxide fuel cell", *International Journal of Hydrogen Energy*, in press.

Arpino, F., Carotenuto, A., Massarotti, N. and Nithiarasu, P. (2008), "A robust model and numerical approach for solving solid oxide fuel cell (SOFC) problems", *International Journal of Numerical Methods for Heat and Fluid Flow*, Vol. 18 Nos 7/8, pp. 811-34.

Arpino, F., Massarotti, N. and Mauro, A. (2010), "A stable explicit fractional step procedure for the solution of heat and fluid flow through interfaces between saturated porous media and free fluids in presence of high source terms", *International Journal for Numerical Methods in Engineering*, in press.

Arpino, F., Massarotti, N., Mauro, A. and Nithiarasu, P. (2009), "Artificial compressibility based-CBS scheme for the solution of the generalized porous medium model", *Numerical Heat Transfer, Part B*, Vol. 55, pp. 196-218.

Autissier, N., Larrian, D.J.V.H. and Favrat, D. (2004), "CFD simulation tool for solid oxide fuel cells", *Journal of Power Sources*, Vol. 131, pp. 313-19.

Bae, J., Lim, S., Jee, H., Kim, J.H., Yoo, Y.S. and Lee, T. (2007), "Small stack performance of intermediate temperature-operating solid oxide fuel cells using stainless steel interconnects and anode-supported single cell", *Journal of Power Sources*, Vol. 172, pp. 100-07.

Beale, S.B., Lin, Y., Zhubrin, S.V. and Dong, W. (2003), "Computer methods for performance prediction in fuel cells", *Journal of Power Sources*, Vol. 118, pp. 79-85.

Bhattacharyya, D., Rengaswamy, R. and Finnerty, C. (2009), "Dynamic modelling and validation studies of a tubular solid oxide fuel cell", *Chemical Engineering Science*, Vol. 64, pp. 2158-72.

Bistolfi, M., Malandrino, A. and Mancini, N. (1996), "The use of different modelling approches and tools to support research activities: an industrial example", *Computers and Chemical Engineering*, Vol. 20, pp. 1487-91.

Brandon, N. and Thompsett, D. (2005), *Fuel Cells Compendium*, Elsevier, Amsterdam.

Campanari, S. and Iora, P. (2004), "Definition and sensitivity analysis of a finite volume SOFC model for a tubular cell geometry", *Journal of Power Sources*, Vol. 132, pp. 113-26.

Cannarozzo, M., Grosso, S., Agnew, G. and Del Borgo, A. (2007), "Effects of mass transport on the performance of solid oxide fuel cells composite electrodes", *Journal of Fuel Cell Science and Technology*, Vol. 4, pp. 99-106.

Celik, I., Pakalapati, S.R. and Salazar-Villalpando, M.D. (2005), "Theoretical calculation of the electrical potential at the electrode/electrolyte interfaces of solid oxide fuel cells", *Journal of Fuel Cell Science and Technology*, Vol. 2, pp. 238-45.

Chan, S.H. and Xia, Z.T. (2002), "Polarization effects in electrolyte/electrode-supported solid oxide fuel cells", *Journal of Applied Electrochemistry*, Vol. 32, pp. 339-47.

Chan, S.H., Khor, K.A. and Xia, Z.T. (2001), "A complete polarization model of solid oxide fuel cell and its sensitivity to the change of cell component thickness", *Journal of Power Sources*, Vol. 93, pp. 130-40.

Costamagna, P. (1997), "The benefit of solid oxide fuel cells with integrated air pre-heater", *Journal of Power Sources*, Vol. 69, pp. 1-9.

Costamagna, P., Magistri, L. and Massardo, A.F. (2001), "Design and part-load performance of a hybrid system based on a solid oxide fuel cell reactor and a micro gas turbine", *Journal of Power Sources*, Vol. 96, pp. 352-68.

Cussler, E.L. (1997), *Diffusion Mass Transfer in Fluid Systems*, Cambridge University Press, Cambridge.

Danilov, V.A. and Tade, M.O. (2009), "A CFD-based model of a planar SOFC for anode flow field design", *International Journal of Hydrogen Energy*, Vol. 34, pp. 8998-9006.

De Benedetti, P.G. and Vayenas, C.G. (1983), "Steady-state analysis of high temperature fuel cells", *Chemical Engineering Science*, Vol. 38, pp. 1817-29.

EG&G Technical Services (2004), *Fuel Cell Handbook*, 7th ed., US Department of Energy Office of Fossil Energy, National Energy Technology Laboratory, Morgantown, WV.

Ferguson, J.R., Fiard, J.M. and Herbin, R. (1996), "Three-dimensional numerical simulation for various geometries of solid oxide fuel cells", *Journal of Power Sources*, Vol. 58, pp. 109-22.

Greene, E.S., Chiu, W.K.S. and Medeiros, M.G. (2006), "Mass transfer in graded microstructure solid oxide fuel cell electrodes", *Journal of Power Sources*, Vol. 161, pp. 225-31.

Hecht, E.S., Gupta, G.K., Zhu, H., Dean, A.M., Kee, R.J., Maier, L. and Deutschmann, O. (2005), "Methane reforming kinetics within a Ni–YSZ SOFC anode support", *Applied Catalysis A: General*, Vol. 295, pp. 40-51.

Hirano, A., Suzuki, M. and Ippommatsu, M. (1992), "Evaluation of a new solid oxide fuel cell system by non-isothermal modeling", *Journal of Electrochemical Society*, Vol. 139, pp. 2744-51.

Ho, T.X., Kosinski, P., Hoffmann, A.C. and Vik, A. (2009), "Modeling of transport, chemical and electrochemical phenomena in a cathode-supported SOFC", *Chemical Engineering Science*, Vol. 64, pp. 3000-9.

Hussian, M.M., Li, X. and Dincer, I. (2007), "Mathematical modeling of transport phenomena in porous SOFC anodes", *International Journal of Thermal Sciences*, Vol. 46, pp. 48-56.

Kakaç, S., Pramuanjaroenkij, A. and Zhou, X.J. (2007), "A review of numerical modeling of solid oxide fuel cells", *International Journal of Hydrogen Energy*, Vol. 32, pp. 761-86.

Kapadia, S. and Anderson, W.K. (2009), "Sensitivity analysis for solid oxide fuel cells using a three-dimensional numerical model", *Journal of Power Sources*, Vol. 189, pp. 1074-82.

Khaleel, M.A., Lin, Z., Singh, P., Surdoval, W. and Collin, D. (2004), "A finite element analysis modeling tool for solid oxide fuel cell development: coupled electrochemistry, thermal and flow analysis in MARC", *Journal of Power Sources*, Vol. 130, pp. 136-48.

Kirubakaran, A., Jain, S. and Nema, R.K. (2009), "A review on fuel cell technologies and power electronic interface", *Renewable and Sustainable Energy Reviews*, Vol. 13, pp. 2430-40.

Li, P.W. and Chyu, M.K. (2005), "Electrochemical and transport phenomena in solid oxide fuel cells", *Journal of Heat Transfer*, Vol. 127, pp. 1344-62.

Lin, C.K., Chen, T.T., Chyou, Y.P. and Chiang, L.K. (2007), "Thermal stress analysis of planar SOFC stack", *Journal of Power Sources*, Vol. 164, pp. 238-51.

Lin, Y. and Beale, S.B. (2006), "Performance predictions in solid oxide fuel cells", *Applied Methematical Modelling*, Vol. 30, pp. 1485-96.

Liu, S., Kong, W. and Lin, Z. (2009), "Three-dimensional modeling of planar solid oxide fuel cells and the rib design optimization", *Journal of Power Sources*, Vol. 194, pp. 854-63.

Lockett, M., Simmons, M.J.H. and Kendall, K. (2004), "CFD to predict temperature profile for scale up of micro-tubular SOFC stacks", *Journal of Power Sources*, Vol. 131, pp. 243-6.

Ma, L., Ingham, D.B., Pourkashanian, M. and Carcadea, E. (2005), "Review of the computational fluid dynamics modeling of fuel cells", *Journal of Fuel Cell Science and Technology*, Vol. 2, pp. 246-57.

Massarotti, N., Nithiarasu, P. and Carotenuto, A. (2003), "Microscopic and macroscopic approach for natural convection in enclosures filled with fluid saturated porous medium", *International Journal of Numerical Methods for Heat & Fluid Flow*, Vol. 13, pp. 862-86.

Massarotti, N., Nithiarasu, P. and Zienkiewicz, O.C. (2001), "Natural convection in porous medium-fluid interface problems", *International Journal of Numerical Methods for Heat & Fluid Flow*, Vol. 11, pp. 473-90.

Morgan, K., Weatherill, N.P., Hassan, O., Brookes, P.J., Said, R. and Jones, J. (1999), "A parallel framework for multidisciplinary aerospace engineering simulations using unstructured meshes", *International Journal for Numerical Methods in Fluids*, Vol. 31, pp. 159-73.

Nishino, T., Iwai, H. and Suzuki, K. (2006), "Comprehensive numerical modeling and analysis of a cell-based indirect internal reforming tubular SOFC", *Journal of Fuel Cell Science and Technology*, Vol. 3, pp. 33-44.

Nithiarasu, P. (2003), "An efficient artificial compressibility (AC) scheme based on the characteristic-based split (CBS) method for incompressible flows", *International Journal for Numerical Methods in Engineering*, Vol. 56, pp. 1815-45.

Palsson, J., Selimovic, A. and Sjunnesson, L. (2000), "Combined solid oxide fuel cell and gas turbine systems for efficient power and heat generation", *Journal of Power Sources*, Vol. 86, pp. 442-8.

Perry, R.H., Green, D.W. and Maloney, J.O. (1997), *Perry's Chemical Engineers' Handbook*, 7th ed., McGraw-Hill, New York, NY.

Riensche, E., Achenbach, E., Froning, D., Haines, M.R., Heidug, W.K., Lokurlu, A. and von Adrian, S. (2000), "Celan combined-cycle SOFC power plant – cell modelling and process analysis", *Journal of Power Sources*, Vol. 86, pp. 404-10.

Riess, I., Gödickemeier, M. and Gauckler, L.J. (1996), "Characterization of solid oxide fuel cells based on solid electrolytes or mixed ionic electronic conductors", *Solid State Ionics*, Vol. 90, pp. 91-104.

Sammes, N. (2006), *Fuel Cell Technology: Reaching Towards Commercialization*, Springer, London.

Singhal, S.C. (2000), "Advances in solid oxide fuel cell technology", *Solid State Ionics*, Vol. 135, pp. 305-13.

Singhal, S.C. and Kendall, K. (2003), *High-temperature Solid Oxide Fuel Cells: Fundamentals, Design and Applications*, Elsevier Advanced Technology, Kidlington.

Standaert, F., Hemmes, K. and Woudstra, N. (1996), "Analytical fuel cell modeling", *Journal of Power Sources*, Vol. 63, pp. 221-34.

Stiller, C., Thorud, B., Seljebo, S., Mathisen, O., Karoliussen, H. and Bolland, O. (2005), "Finite-volume modeling and hybrid-cycle performance of planar and tubular solid oxide fuel cells", *Journal of Power Sources*, Vol. 141, pp. 227-40.

Sundén, B. and Faghri, M. (2005), *Transport Phenomena in Fuel Cells*, WIT Press, Southampton.

Vayenas, C.G., De Benedetti, P.G., Yentekakis, I. and Hegedus, L.L. (1985), "Cross-flow, solid-state electrochemical reactors: a steady-state analysis", *Industrial and Engineering Chemistry: Fundamentals*, Vol. 24, pp. 316-24.

Whitaker, S. (1961), "Diffusion and dispersion in porous media", *AIChE Journal*, Vol. 13, pp. 420-7.

Xue, X., Tang, J., Sammes, N. and Du, Y. (2005), "Dynamic modelling of a single tubular SOFC combining heat/mass transfer and electrochemical reaction effects", *Journal of Power Sources*, Vol. 142, pp. 211-22.

Yakabe, H., Hishinuma, M., Uratani, M., Matsuzaki, Y. and Yasuda, I. (2000), "Evaluation and modeling of performance of anode-supported solid oxide fuel cell", *Journal of Power Sources*, Vol. 86, pp. 423-31.

Zhao, F. and Virkar, A.V. (2005), "Dependence of polarization in anode-supported solid oxide fuel cells on various cell parameters", *Journal of Power Sources*, Vol. 141, pp. 79-95.

Zhu, H. and Kee, R.J. (2003), "A general mathematical model for analyzing the performance of fuel-cell membrane-electrode assemblies", *Journal of Power Sources*, Vol. 117, pp. 61-74.

Zienkiewicz, O.C., Taylor, R.L. and Nithiarasu, P. (2005), *The Finite Element Method for Fluid Dynamics*, Elsevier, Oxford.

Corresponding author
A. Mauro can be contacted at: alessandro.mauro@uniparthenope.it